



# Evaluation of pigment distribution in contact lenses with iris patterns by multiprobe analysis methods

Eri Ito <sup>1,2</sup> · Hiroshi Takase<sup>3</sup> · Katsuhiro Yamamoto <sup>1</sup>

Received: 23 March 2023 / Revised: 9 May 2023 / Accepted: 29 May 2023 / Published online: 25 July 2023  
© The Author(s) 2023. This article is published with open access

## Abstract

Iris-patterned lenses have recently become popular in the field of soft contact lenses (SCLs), and SCLs are typical examples of an industrial application of gel materials. As these patterns can be printed using oxidized-metal-containing pigments, the oxidized metals may be exposed on the lens surface depending on the printing method, potentially accounting for various health hazards. To evaluate the state of the exposed oxidized metal on the lens surface, we analyzed the colored layer, mainly consisting of pigments, on the lens surface via multiple probing methods, such as transmission electron microscopy (TEM), scanning TEM with energy-dispersive X-ray spectroscopy, hard X-ray photoelectron spectroscopy, and X-ray absorption fine structure (XAFS). Furthermore, we confirmed that the XAFS conversion electron yield (CEY) and fluorescence yield (FY) methods demonstrated high sensitivity toward revealing the existence of pigments. Thus, the use of a combination of XAFS CEY and FY methods can facilitate the effective distribution analysis of various elements in the interior of materials such as cosmetic CLs.

## Introduction

Polymers have been employed in industrial fields as materials for satisfying societal needs, and materials exhibiting three-dimensional (3D) cross-linked network structures have long been utilized in such fields [1, 2]. Furthermore, studies abound on the utilization of gels as solvated products in 3D cross-linked polymers [3]. Among them, hydrogels solvated in water or aqueous solutions can be applied in medical devices [4].

As a hydrogel-based medical device, soft contact lenses (SCLs) have been in existence for more than 50 years [5]. This medical device is worn on the cornea for vision correction and exploits the surface tension of tear fluid. This medical device is widely used in daily life. Following the invention of the water-adsorbent material 2-hydroxyethyl methacrylate (HEMA) and its polymerized form poly(HEMA), various gel-based materials have been developed for SCLs. Compared with resin-based CLs (e.g., poly(methyl methacrylate)), hydrogel-based SCLs can exhibit better flexibility and comfort because of their water content and their higher affinity for tears on the lens surface. However, to improve oxygen permeability, silicone hydrogel CLs, which are fabricated from the copolymers of silicone compounds, as well as water-absorbent materials, have been in practical use since 2000 [6]. However, along with their excellent bulk performance, silicone hydrogel materials are also difficult to surface control. Therefore, it is crucial to analyze the relationship between the chemical structures and surface properties of polymeric materials [7] as well as the behavior of water near biomaterial interfaces [8].

Conversely, gel material-based CLs are also used for “cosmetic” purposes, for example, in altering eye color or enlarging its appearance. Thus, these CLs are called “cosmetic CLs (CCLs)” [9]. The use of CCLs generally began in

**Supplementary information** The online version contains supplementary material available at <https://doi.org/10.1038/s41428-023-00810-8>.

✉ Eri Ito  
ito.eri@nitech.ac.jp

<sup>1</sup> Department of Life Science and Applied Chemistry, Graduate School of Engineering, Nagoya Institute of Technology, Gokisocho, Showa-ku, Nagoya 466-8555, Japan

<sup>2</sup> Menicon Co. Ltd., 3-21-19 Aoi, Naka-ku, Nagoya 460-0006, Japan

<sup>3</sup> Core Laboratory, Nagoya City University Graduate School of Medical Sciences, 1 Kawasumi, Mizuho-cho, Mizuho-ku, Nagoya 467-8601, Japan

the 1990s and involved the printing of iris patterns using ink containing pigments on a part or on the entire area overlapping the cornea of the lens [10]. In other words, CCLs are printed using pigments (i.e., inorganic substances) that are dispersed near the surface of the gel material.

Lens coloring has a long history, and the coloring of entire lenses has long been widely used to improve their operability [11]. Synthetic organic dyes, which dissolve in the raw materials of lenses and form a chemical bond with the material via a polymerization reaction, are often used as colorants for handling tints. In contrast, pigments are often used as colorants for CCLs [11]. Numerous gel lenses are now produced via mold polymerization. The raw material is poured into a resin mold and exposed to heat or light energy to initiate the polymerization reaction. Before mold polymerization, the mold is printed into patterns using ink-containing pigments. Afterward, the mold can be used to produce CCLs by fixing the colored layer simultaneously with the polymerization of the raw material [12]. Products of various types and designs are sold, and it is reported that the number of CCL users in some areas exceeds 30% of all CL users [13]. Most of these users are young, and case-control studies have revealed that the risk of infection is 16.5 times higher among CCL wearers than among those who only wear lenses for refractive correction [14]. This is because of the failure of users to follow the established wear schedule, as well as the low qualities of CCLs [9, 15]. Despite the development of new, safe materials, such as silicone hydrogel materials, most CCL are still fabricated using poly(HEMA) material because of the facile manufacturing process. There are also reports of issues relating to color-layer qualities, as the colored layers of lenses with exposed pigments on their surfaces exhibit microbial adhesion, becoming allergy triggers [16]. Regarding the color-layer quality, the National Consumer Affairs Center of Japan reported that some lenses contained exposed pigments on their surfaces [17].

Thus, the quality of the colored layer of CCLs, i.e., the position of the colored layer in relation to the lens surface in contact with the human body along the thickness direction, presents an issue; therefore, the pigment position is a crucial factor in ensuring safety [13, 18]. Fig. 1 shows a real example of CCLs. It is impossible to determine if the pigment-containing printed layer is exposed on the lens surface by visual appearance alone. The objective of our study was to address this issue.

To do this, several surface-analysis methods have been implemented, beginning with the primitive-surface-wiping method using cotton swabs and including scanning electron microscopy (SEM), atomic force microscopy, and time-of-flight secondary ion mass spectrometry [17, 19–21]. However, no standardized evaluation method has been

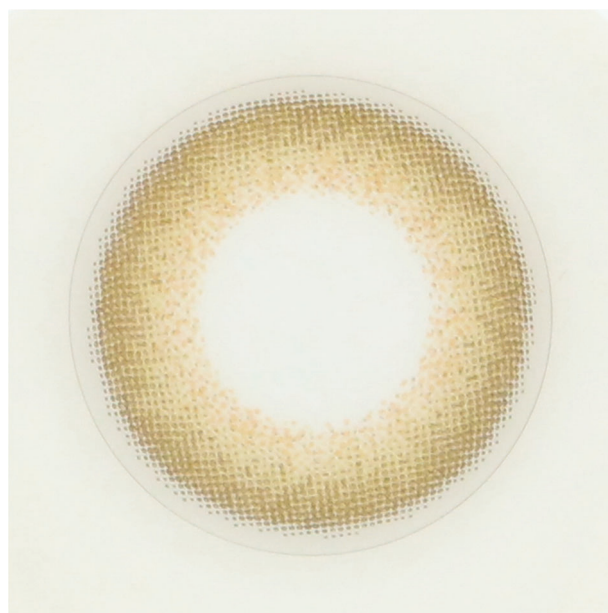


**Fig. 1** Example of the appearance of a CCL. An iris pattern is printed on the CCL. Although various designs, colors, printing areas, and printing methods are employed commercially, CCLs generally have the shown appearance

established for obtaining the location and detailed information of the colored layer on CCLs, i.e., the distribution area and form of pigments. Conversely, the incidences of anterior segment disorders caused by the use of CCLs continue to increase. Depending on the manufacturing method, this colored layer is printed on the eyelid conjunctiva or cornea side. However, in either case, lenses containing pigment components that are exposed on the surface are prone to causing anterior segment disorders.

To analyze the position and distribution depth of the pigments that are dispersed in gel lenses, we prepared ultrathin sections of the colored layer of CCLs and observed them via transmission electron microscopy (TEM) [22], confirming the distribution and position of the pigments in the CLs. Based on the results, we analyzed the distribution form and shape of the pigment particles and classified the lenses based on their distribution characteristics. This method allows visualization of pigment exposure on the lens surface. Furthermore, an understanding of the depth and morphology of pigment distribution from the topmost layer of the lens surface revealed the depth and scale for measurements along the thickness direction of the lens, narrowing down the areas to investigate, thereby allowing for a determination of the quality of the colored layers of CCLs. Put differently, it became possible to narrow the to-be-observed area to determine the quality of the colored layer of CCLs [23–29]. However, a technical hurdle exists in the preparation of ultrathin section samples for the TEM observation of SCLs.

To further elucidate the colored layer in which inorganic substances are dispersed, the elemental composition of the

layer must be understood. Iron oxides represent the general inks for generating the colored layer of CCLs; however, in reality, iron oxide, chromium oxide, phthalocyanine organic pigments, natural pigments, and titanium oxide are used to accentuate red, green, blue, yellow, and white colorations, respectively [12]. Organic dyes, such as phthalocyanine, have long been used in handling tints and dissolution in raw materials; they are chemically immobilized via polymerization reactions [11]. In contrast, pigments comprising oxidized metals, such as iron oxides, do not dissolve in the raw materials, and TEM observations have confirmed that they exist as agglomerates. Previous analyses revealed the presence of chlorine, titanium, and iron [19], although the relationship between the detected elements and their positions has not been clarified. Therefore, in this study, scanning TEM (STEM) was combined with energy-dispersive X-ray spectroscopy (EDS), STEM-EDS, to analyze the elemental composition of the pigment present in the colored layer of CCLs.

As mentioned above, TEM is an effective tool for clarifying the location of the pigment-containing area, although it is challenging to manually prepare ultrathin film sections of the lenses, rendering TEM unsuitable for large-scale evaluations. Therefore, we employed photoelectron spectroscopy (PES), which is conventionally employed for surface analyses of the elemental compositions and chemical states of materials. Furthermore, we performed soft X-ray PES (SoXPES) and hard XPES (HAXPES), which can be used to measure the top layer of a sample and nondestructively analyze deeper regions to reveal the elemental compositions of the colored layers of CCLs.

In addition to HAXPES, X-ray absorption fine structure (XAFS) spectroscopy represents an elemental analysis method that utilizes synchrotron radiation X-rays [30]. XAFS comprises multiple detection methods, which can be combined to ensure in-depth analyses [31]. Therefore, we applied the conversion electron yield (CEY) and fluorescence yield (FY) methods of XAFS (CEY-XAFS and FY-XAFS, respectively) to determine the elemental trends in the colored layers of CCLs.

CLs are regarded as a highly successful industrial application of polymer gels, which are three-dimensional cross-linked polymers. CCLs are particularly popular among young people and have inorganic pigments printed near the lens surface layer. The safety of CCLs is closely related to whether these pigments are exposed at the surface. However, no method has been established for detecting the presence or absence of pigment exposure on the CCL surface, and the establishment of such a method remains an important issue. Herein, we performed complementary analyses using multiple probes: TEM, which has been used to analyze the surface (local) structure of polymers; HAXPES, which has recently been used to analyze the surface chemical structure of polymers; [32] and XAFS, which has a proven track record in the surface analysis of metallic materials by employing the CEY (surface sensitive) and FY

(bulk sensitive) methods. Our aim was to clarify the distribution and chemical composition of inorganic substances dispersed in commercially available CCLs, visualize the actual distribution of the printed layer, and develop safety guidelines for CCLs with regard to pigment distribution in the printed layer.

## Experiment

### Materials

We employed the following commercially available CCLs as our samples:

Sample 1: CL ISO [33] classification: Group I, water content: 38%

Sample 2: CL ISO classification: Group IV, water content: 58%.

Notably, previous studies revealed that the pigments in Samples 1 and 2 are exposed and not exposed on the lens surface, respectively [23]. Each CCL was removed from the shipping solution in the lens case, immersed in distilled water, and utilized for the experiment. The lens curvatures on the eyelid conjunctiva and cornea sides were called the front curve (FC) and base curve (BC), respectively. Pigment printing is typically applied to the FC or BC surface of CCLs; thus, we observed the printed surfaces.

### Measurements

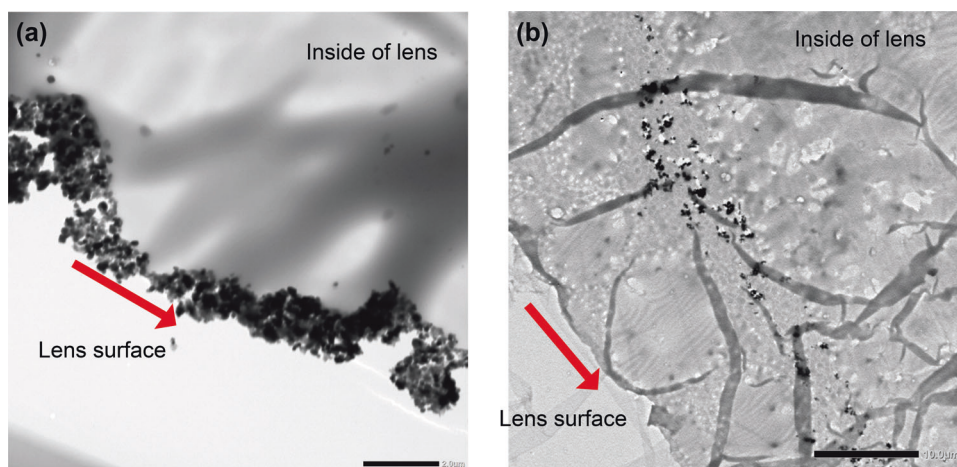
#### TEM

A rectangular printed area of 3 mm × 0.5 mm was cut out from a sample that had been removed from distilled water using a razor. The apparatus, a cryo unit (Leica FC7: Leica Microsystems) that was attached to an ultramicrotome (Leica UC7: Leica Microsystems), was adjusted to  $-80\text{ }^{\circ}\text{C}$  to  $-100\text{ }^{\circ}\text{C}$  using liquid nitrogen. The sample pieces were frozen in the gas phase inside the cryo unit. A glass or diamond knife (Syntek Co., Ltd.) was employed to prepare ultrathin sections of the printed area of the cross-section of the sample (the thickness of the cut sample was  $\sim 100\text{ nm}$ ). The sections were placed on a carbon-coated copper grid comprising a collodion support film for TEM observation. The ultrathin sections on the grid, as obtained via these procedures, were observed under a transmission electron microscope (JEM-1400Plus; JEOL Ltd.) at an acceleration voltage of 100 kV without staining.

#### STEM-EDS

The prepared ultrathin sections (see “TEM”) were analyzed via STEM-EDS (JEM-2800; JEOL Ltd.) at an acceleration voltage of 200 kV and a magnification of 100,000–300,000 times.

**Fig. 2** TEM images of the lens cross-section in the thickness direction of the colored layer: (a) Sample 1 (scale bar = 2.0  $\mu\text{m}$ ) and (b) Sample 2 (scale bar = 10  $\mu\text{m}$ ). The arrows indicate the lens surfaces



### SoXPES

The SoXPES measurements were conducted on a fully automated XPES system (K-Alpha+; Thermo Fisher Scientific K.K.) with an Al K-Alpha X-ray source at a pass energy of 200 eV, a dwell time of 25 ms, and an energy step of 1.0 eV. The distilled water-displaced samples were dried, after which the printed area was cut into 5 mm  $\times$  5 mm squares. Finally, wide scans were performed in the energy range of  $-10$  to 1350 eV.

### HAXPES

The HAXPES measurements were conducted on a HAXPES instrument (R-4000; Scienta Omicron, Inc.) that was at BL46XU in SPring-8. The excitation X-rays were monochromatized to  $\sim 8$  keV, and an electron analyzer (R-4000; Scienta Omicron, Inc.) was used. The measurements were conducted at 25  $^{\circ}\text{C}$ , with a pass energy of 200 eV and a slit curvature size of 0.5 mm, and the photoelectron takeoff angles (TOAs) were 15 $^{\circ}$  and 80 $^{\circ}$ . The distilled water-displaced samples were dried, cut into 8 mm  $\times$  1 mm rectangles, and coated with a few nanometers of osmium before measurements to prevent charging on the surface.

### XAFS

The XAFS measurements were conducted at BL551 (Figure S1 in the Supporting Information (SI)) of the Aichi Synchrotron Radiation Center using the FY (bulk sensitive) and CEY (surface sensitive) modes. Fluorescence X-rays emitted from the sample were detected using a seven-element silicon drift detector with a micrometer-order probing depth. For the CEY method, the XAFS spectrum was detected using the sample drain current. Typically, the probing depth is much smaller than the penetration depth of the incident X-rays. The XAFS spectra were measured in the energy

region of 4.67–8.81 keV across the Ti K-edge ( $\sim 4.97$  keV) to the Co K-edge ( $\sim 7.71$  keV) using the step-scanning method. Continuous X-rays from the light source were measured by a Si(111) double-crystal monochromator, and the measurements were conducted under a helium atmosphere.

## Results & discussion

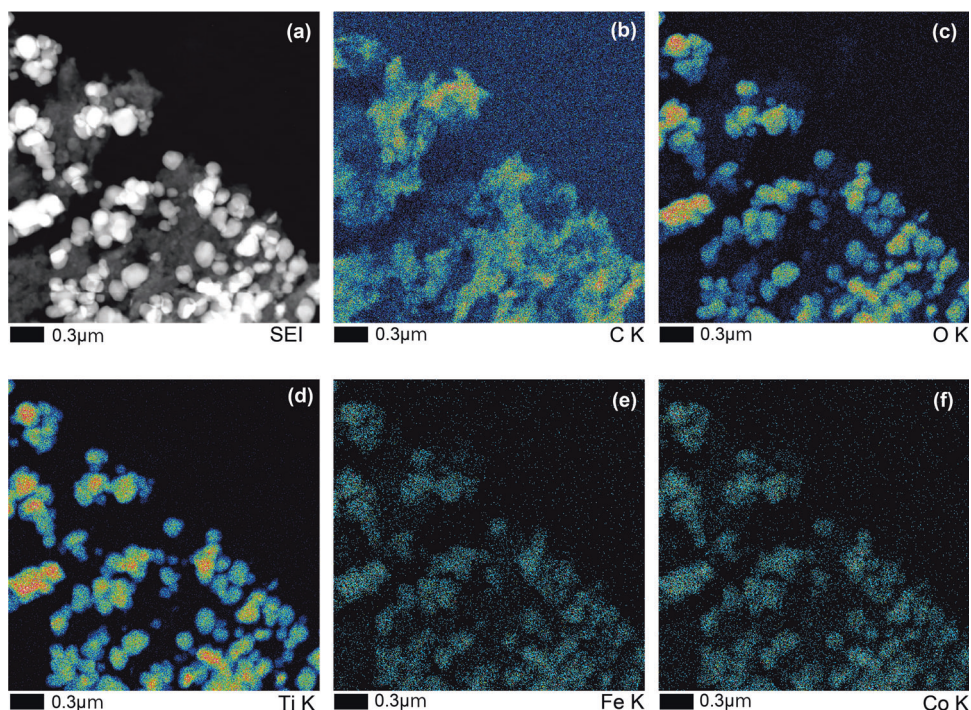
### Distribution morphology and elemental analysis of the pigment particles in the lenses by TEM and STEM-EDS measurements

Figure 2a, b show the results of TEM observations of the ultrathin film sections of Samples 1 and 2, respectively. The estimated diameter of the smallest pigment-particle unit in the colored layer was  $\sim 100$  nm. The pigments in Sample 1 appeared to exist as agglomerates near the lens surface, and the pigments were significantly exposed at the lens surface. They exhibited an area of  $\sim 1$   $\mu\text{m}$  in depth from the topmost lens surface layer, which could be the colored layer. Conversely, although Sample 2 contained pigment agglomerates with a maximum sub $\mu\text{m}$  size, the pigments were dispersed over a wide area, and the distribution area was 15–20  $\mu\text{m}$  in the depth direction from the surface. Regarding the morphology of the colored layer of the CCLs, Sample 1 exhibited a typical structure in which the pigment was exposed, whereas Sample 2 exhibited a sandwich structure. We assumed that both structures were derived from the color-layer-formation method.

Furthermore, Fig. 3 shows the results of the elemental analysis of the pigment particles via STEM-EDS measurements of the agglomeration site of Sample 1 particles. Figure 3a shows the SEM image in the secondary electron imaging (SEI) mode, as obtained via the measurement, and the white areas indicate the pigment particles: O, Ti, Fe, and Co (Fig. 3c, d, e, and f, respectively) were present at



**Fig. 3** STEM–EDS images of Sample 1. **(a)** SEM image in the SEI mode, where the white areas indicate the pigment particles. Distributions of **(b)** carbon, **(c)** oxygen, **(d)** titanium, **(e)** iron, and **(f)** cobalt



significant levels, overlapping with the white areas in the SEI. The signal corresponding to titanium was most clearly observed in the area where the pigment particles were concentrated; iron and cobalt were also observed in overlapping positions. Additionally, the distribution of carbon, which is a constituent of the material, was observed regardless of the presence of particles, although some signals overlapped with the location of particles. The signal corresponding to oxygen was stronger than that corresponding to carbon, and it overlapped with the distributions of titanium and iron. Although it is known that iron oxide is mainly employed in CCLs [10], the results of the STEM–EDS measurement of the particle part of this lens indicated that titanium, rather than Fe, was strongly present in the particle-agglomeration area. This signal was significant in the particle agglomerates. Conversely, Fe and Co exhibited relatively low concentrations, overlapping with the Ti-distribution region and strongly indicating that these particles were pigments. Furthermore, the oxygen-atom distribution overlapped with Ti and Fe, indicating that the particles consisted of pigmented iron oxide or titanium oxide. Carbon atoms were also observed in the pigment-particle sites, indicating that the pigments were coated with polymers or organic molecules.

### Near-surface composition analysis via XPES

The colored (tinted) and transparent (clear) areas on the surface of the CCLs were analyzed via SoXPES, a standard method for performing surface elemental analysis, and the

results revealed the presence of polymer-derived elements, such as  $O_{1s}$  and  $C_{1s}$ , although no peaks corresponding to metallic elements, such as Fe and Ti, were observed (Fig. S2 in SI).

The following procedure was employed to validate the measured depth–thickness of lens materials exhibiting different thicknesses for different TOAs in the HAXPES experiment at SPring-8 BL46. A homopolymer, poly(3-(methacryloyloxy)propyl tris(trimethyl silyloxy)silane) (PMPTS), which is a typical lens component, was cast on a silicon substrate using different polymer concentrations of a tetrahydrofuran solution, as well as by changing the speed of the spin coater. The thickness of the PMPTS film was measured via ellipsometry. The sample preparation is explained in the SI. The detectable, real measurement depth of each TOA was estimated at SPring-8 BL46 by preparing different thicknesses of the PMPTS thin films. The osmium coating was unnecessary for a spin-coated film on the silicon wafer because it is rapidly discharged from the sample via the wafer. At a TOA of  $80^\circ$ , the photoelectrons from the  $Si_{1s}$  orbital of the Si–Si bond of the silicon substrate could be detected in the sample with a thickness of 110 nm. The photoelectron of  $Si_{1s}$  was almost undetectable when the thickness was 124 nm, indicating that photoelectron information can be obtained at a maximum (limitation) depth of  $\sim 120$  nm from the surface to the interior direction for PMPTS (Fig. S3 in SI). Generally, for polymeric materials, the analytical depth from the surface,  $d$ , is calculated using  $3\lambda$ , which is three times the inelastic mean free path (IMFP  $\lambda$ ) of the electrons. For SoXPES using the  $AlK\alpha$  line, the

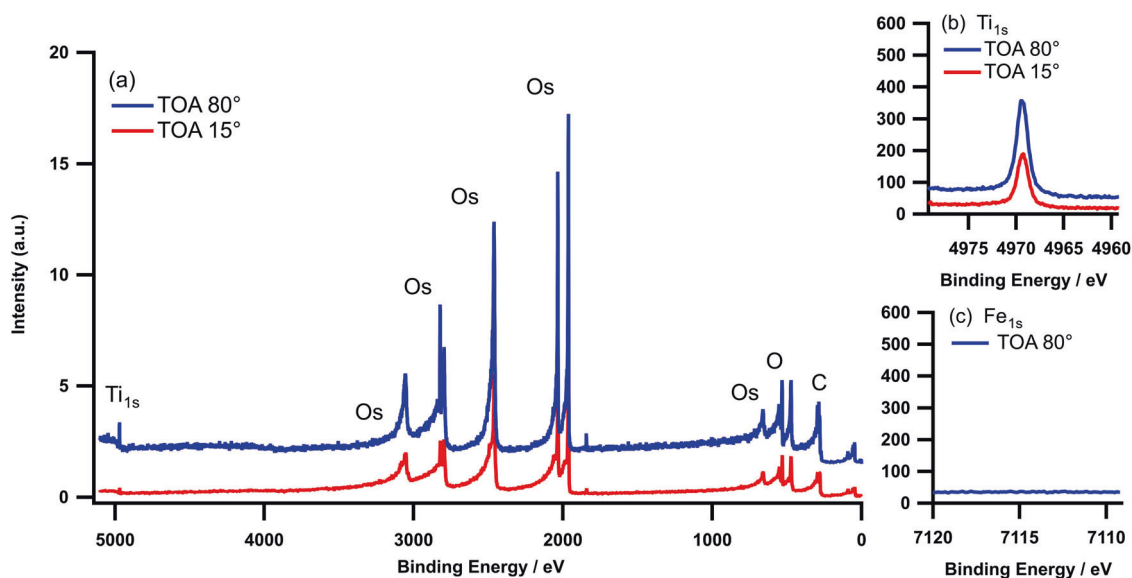


**Fig. 4** HAXPES measurements of Sample 1 at different TOAs: (a) wide and (b, c) narrow scans related to  $\text{Ti}_{1s}$  and  $\text{Fe}_{1s}$ , respectively. The  $\text{Ti}_{1s}$  spectra were observed at TOAs of 15° and 80°, while the  $\text{Fe}_{1s}$  spectra were not confirmed at 80°. Notably, many signals from

osmium were detected in the wide-scan spectrum (a) because of the osmium coating that was applied to the sample surface to prevent charging

analytical depth is given by  $\lambda = 3 \text{ nm}$  for the polymer compounds, which is given by  $d = 3\lambda \sin\theta$  ( $\theta = \text{TOA}$ ) [34, 35].  $d$  for HAXPES (8 keV) was 14–15 nm [36]. The analytical depths were approximately 10 and 45 nm for TOAs of 15° and 80°, respectively. The depth of detection from the surface, which is shown here, is sufficiently high considering that the depth of the detection limit at  $\theta = 15^\circ$  is estimated from the measurement results at  $\theta = 80^\circ$ , which attenuates in proportion to  $\sin\theta$  [37], and the estimated depth is  $\sim 30 \text{ nm}$ .

Figure 4 shows the results of the wide (a) and narrow (b and c) scans ( $\text{Ti}_{1s}$  and  $\text{Fe}_{1s}$ ) of Sample 1 via HAXPES. Numerous osmium-related signals were detected in the wide-scan spectrum (a) because of the osmium coating that was applied to the sample surface to prevent charging; moreover, the thickness of the osmium coating was 1–2 nm, which was confirmed using the osmium coating on a silicon wafer with identical coating conditions (see SI). Figure 4b shows that the signal of the  $\text{Ti}_{1s}$  component was observed at TOAs of 15° and 80° for Sample 1. The binding energy (BE) of the  $\text{Ti}_{1s}$  component was 4969 eV, which was attributed to titanium oxide [38]. Although iron oxide was considered the main pigment component, no  $\text{Fe}_{1s}$  signals were detected at a TOA of 80° (Fig. 4c). Conversely, for Sample 2, no  $\text{Fe}_{1s}$  or  $\text{Ti}_{1s}$  signals were observed in the narrow scan, although the  $\text{O}_{1s}$  and  $\text{C}_{1s}$  peaks were observed in the wide scan (Fig. S4 in SI).

As the surfaces of CCLs are generally printed in brown, black, or gray colors, their pigment components could be Fe, Cr, or Co, which exhibit those colors. The STEM–EDS results revealed that Fe and Co were also present, although

Ti was predominant. However, Fig. 4 shows that only the  $\text{Ti}_{1s}$ -related signal was detected at all TOAs. It is known that titanium dioxide enhances the white color in printing and is used to accentuate whiteness [12]. Although Fe- and Cr-based colorations are readily considered to be detected via STEM–EDS, the HAXPES measurements revealed the existence of only titanium oxide. Why was only Ti observed and not Fe, Co, or Cr? The STEM–EDS results indicated that the ratio of Ti was overwhelmingly high, complicating the detection of Fe or Co. Alternatively, Fe and Co signals were not observed because the Ti component covered the surface of each pigment particle (iron oxide) with a certain thickness. Based on the ratios of the STEM–EDS components, we anticipated that the Fe signal would be detectable via HAXPES. Therefore, the pigment particles might exhibit a titanium oxide-covered structure.

$\text{Ti}_{1s}$ ,  $\text{Fe}_{1s}$ , and the other pigment-derived elements were not observed in the surface layer of Sample 2. The TEM observation revealed the presence of Fe in the region that was inaccessible using HAXPES. Therefore, only light elements, such as C, O, and N, which were derived from the lens polymer, were observed.

By verifying the analytical depth of the PMPTS thin films, we observed that depth information (detection limits) was obtained up to  $\sim 30$  and 120 nm from the outermost surface when measured at  $\theta = 15^\circ$  and  $80^\circ$ , respectively. Directly quantifying the analytical depth of the HAXPES measurements using commercially available contact lenses was very difficult. However, most CCLs had a composition similar to that of PMPTS. As IMPF does not change considerably for polymeric materials, it is safe to assume that

the analytical depth for the lens materials was almost the same as that estimated for PMPTS. However, when additional pigments (metallic elements) exist in the measurement area, the density of the pigments is expected to be much higher than that of the polymer material, and photoelectrons are unlikely to be capable of traveling through the high-density region (lower levels of emission). When X-rays of 8 keV were used for HAXPES, the IMFP  $\lambda$  of the electrons in the polymeric materials was 14–15 nm, as mentioned above. Conversely, the estimated titanium dioxide  $\lambda$  was  $\sim 10$  nm [39, 40], and the analytical depth could be lower in the pigment regions. Therefore, the photoelectron information in this study was obtained using an analytical depth of  $\sim 45$  nm (up to ca. 120 nm) for Sample 2 if only the polymer compounds were utilized. In Sample 1, many titanium dioxide particles were observed on the sample surface, indicating that the analytical depth  $\lambda$  could be  $\sim 30$  nm considering the titanium dioxide  $\lambda$ . Iron was not detected, and this indicated that the iron oxide particles were coated with titanium oxide layers of thicknesses of several tens of nanometers.

SoXPES (Soft X-ray AlK $\alpha$ ) is conventionally employed for surface analysis. In the SoXPES measurement, neither Ti nor Fe photoelectrons were detected in Sample 1 (Fig. S2) because the surface of the pigment particles was thinly covered by the polymers and organic components that were employed as binders between the particles and lens material. Although the STEM–EDS observations could not determine the thickness (coverage) of the polymeric materials, their detection of carbon elements near the pigment component (Fig. 4c) demonstrated that they were coated with organic molecules. As the analytical depth in the SoXPES measurement of soft materials is only a few nanometers, the pigment components (Ti and Fe) could not be detected via traditional SoXPES measurement even when the pigment particles were segregated on the surface (Sample 1), and this is because of the existence of ultrathin organic components near the surface of the pigments.

### Detection of pigment components via XAFS measurements

The CEY and FY modes of XAFS are generally employed to obtain the X-ray absorption spectra of elements from the surface to approximately 100 nm (surface sensitive approach) and a few micrometers from the surface (bulk sensitive approach), respectively, although the depths depend on the target sample. We conducted XAFS measurements in the hard X-ray region, including the Fe and Ti absorption edges. Figures 5 and 6 show the measurement results of Samples 1 and 2, respectively.

Figure 5 shows that the CEY mode only confirmed the Ti K-edge (4985 eV, titanium oxide [30]). In contrast, the FY

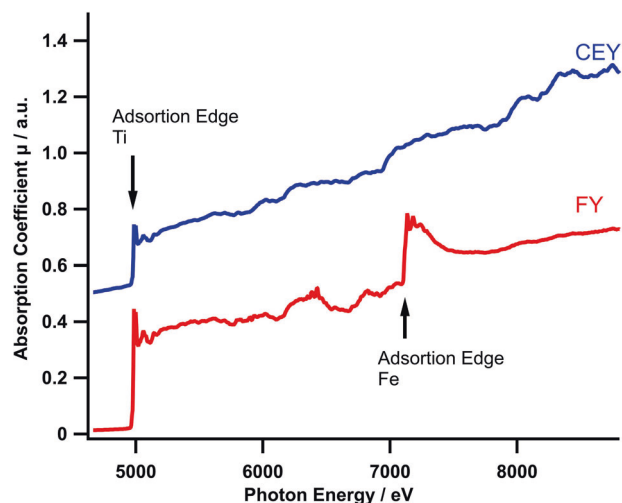


**Fig. 5** XAFS spectra for Sample 1 detected in the CEY and FY modes. In both modes, the adsorption edge of titanium oxide was observed at 4985 eV, whereas that of iron oxide was observed at 7085 eV only in the FY mode

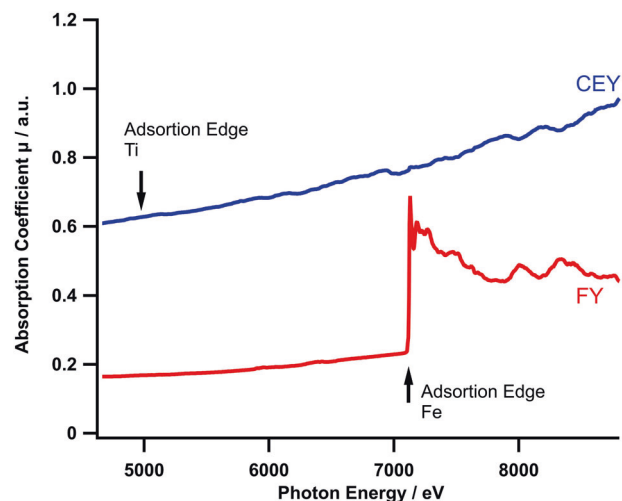


**Fig. 6** XAFS spectra of Sample 2 detected in the CEY and FY modes. In CEY mode, no adsorption edges related to Ti and Fe were observed in the measurement region; however, in FY mode, only the K-edge of iron oxide (7085 eV) was observed

mode confirmed the Ti and Fe K-edges (7085 eV, iron oxide [41]). This indicated that the Ti and Fe components in Sample 1 existed in the shallow and deep regions from the surface, respectively, which is in good agreement with the results of HAXPES showing only Ti<sub>1s</sub> photoelectrons.

Conversely, using the CEY mode, which is particularly useful for near-surface analysis, Ti, Fe, and other metallic elements, such as Co and Cr, were not confirmed in Sample 2 (Fig. 6). However, Fe was confirmed in the FY mode, which enables measurements of deeper regions (the entire film). Therefore, we inferred that no metallic components existed on the surface of Sample 2, although Fe-containing components were utilized. This result is also consistent with



that obtained via HAXPES. The distribution of the metal elements on the top surface and inside Samples 1 and 2, as determined from these elemental analyses, agrees with the distribution trend in the particles in Fig. 2.

TEM allowed us to directly confirm the distribution of pigments used in printing CCLs. Elemental analysis using STEM–EDX allowed us to observe the presence of Fe, Ti, and Co as well as O. The presence of O was attributed to iron oxide, which is widely used in CCLs, and other metallic oxides. TEM observations provided the distribution of the printed layer in CCLs (i.e., whether or not the pigments were present in the topmost surface of the lens). Moreover, TEM observation was very useful for determining the degree of pigment agglomeration as well as confirming their elemental distributions. However, preparing ultrathin sections of soft gel materials requires considerable technical skills. This can take a substantial amount of time, especially when many samples need to be analyzed. Therefore, we used synchrotron radiation analysis in an attempt to nondestructively and quickly analyze elements in the samples. For CCLs that TEM confirmed to have pigments exposed on the surface, HAXPES provided the Ti 1s range, which is inaccessible with SoXPES, and revealed the presence of Ti near the surface. Furthermore, a combination of CEY and FY-XAFS confirmed the presence of Fe, which is a typical constituent of pigments, as well as Ti in the topmost surface layer. CEY and FY-XAFS have high measurement sensitivity and can be used to detect elements that cannot be detected using XAFS at low concentrations. The synchrotron experimental results suggest that the distribution of pigments on the topmost surface can be detected by using the signal of Ti, Fe, or other metals as indicators. This approach requires the X-ray energy range to include the adsorption edges of the target elements. For a more effective approach and precise analysis, TEM observation can be performed only on CCLs screened by synchrotron observations to potentially have pigments exposed on the surface.

We suggest that CCLs containing pigments on the topmost surface layer may be selected by first applying HAXPES and CEY-XAFS instead of TEM.

Thus, the complementary use of multiple probes revealed the location and elemental composition of inorganic pigments in the polymeric materials. We believe that this approach provides a solution to the urgent problem of identifying the location of the printed layer to ensure the safety of CCLs.

## Conclusion

In this study, we performed electron microscopy to observe the morphologies of two types of CCLs exhibiting different

pigment-distribution states. Additionally, we examined a method for detecting the distribution states of both pigment components, followed by their elemental and surface analyses.

In Sample 1, the observation-based particle size, as estimated via TEM, was 100–300 nm, and particles exhibiting this size were present as agglomerates. The STEM–EDS measurements revealed that Fe and Co existed in the Ti-distributed areas. The high oxygen concentration of the region with these metals further indicated that the particles were metal oxides. The HAXPES measurements revealed that titanium oxide existed near the surface of the lens material, but iron oxide was not detected. Furthermore, CEY-XAFS revealed that titanium oxide was present near the surface, and FY-XAFS revealed the presence of iron and titanium oxides. The absorption edges (XAFS) and BEs (HAXPES) further revealed that the detected metallic elements were oxidized metals, supporting the high concentration of oxygen atoms around the Fe, Co, and Ti elements that were observed via STEM–EDS measurements. Furthermore, these findings indicated that Ti was present on the surface of the particles in Sample 1, i.e., the iron oxide was coated with titanium oxide.

For Sample 2, the TEM observations confirmed that the diameter of the particles of constituent units was comparable with that of Sample 1. The particles were widely distributed and located at  $\geq 15 \mu\text{m}$  primarily along the interior direction of the lens surface, although agglomerations of several micrometers were observed in some areas. Therefore, the SoXPES, HAXPES, and hard X-ray XAFS measurements confirmed the presence of polymeric components in the surface layer and metallic oxides in the printed layer in the interior of the lens.

Although various health hazards are associated with CCLs, the safety of the lens surface was discussed based on surface pigment exposure, and the establishment of a method for detecting pigment exposure on the lens surface remains an urgent issue. Therefore, we verified the correlation between the elemental composition and elemental distribution of the particles in the CCLs. The depth and distribution trends in the target elements were obtained in this study; therefore, these surface analysis methods can be combined to establish an evaluation method for pigment exposure in CCLs. For the CCLs, we confirmed that the elements on the deeper side, inaccessible via SoXPES, which is conventionally employed for surface analysis, can be detected via synchrotron radiation HAXPES and XAFS. Additionally, we confirmed that CEY-XAFS and FY-XAFS methods could be combined as a practical approach for revealing the depth-based elemental distribution of materials such as CCLs.

Moreover, new CCLs are continuously being released with different brands and designs, which necessitates the



establishment of a system that can provide comprehensive safety information regarding the printing layers of these CCLs, even for commercial lenses for which the data on the printing inks and methods are unknown. To achieve this, we aim to establish strategies that would ensure the accurate evaluation of numerous lenses by screening lenses based on their elemental distribution trends on the surface and interior using multiple evaluation methods, such as XAFS, which was employed in this study, followed by TEM and STEM–EDS observations of lenses, which must be confirmed in detail.

**Acknowledgements** The synchrotron radiation experiments were performed at BL46XU in SPring-8 with the approval of RIKEN (proposal no. 2019A1779, 2019B1871, 2019B1910, 2020A1639, 2020A1741, 2021A1566). The XAFS experiments were conducted at BL5S1 of the Aichi Synchrotron Radiation Center, the Aichi Science & Technology Foundation, Aichi, Japan (proposal no. 202204082). We thank Dr. Satoshi Yasuno (JASRI) for his guidance and support for the HAXPES measurements at SPring-8 and are grateful to Dr. Osamu Fukuoka (Aichi Synchrotron Radiation Center) and Dr. Toshiaki Hiroto (SPring-8 service) for their guidance and support for the Aichi-SR XAFS measurements. We acknowledge Ms. Atsuko Mori (technical staff at the Nagoya Institute of Technology) for her support in the STEM–EDS measurements. The authors would like to thank Enago ([www.enago.jp](http://www.enago.jp)) for the English language review.

## Compliance with ethical standards

**Conflict of interest** The authors declare no competing interests.

**Publisher's note** Springer Nature remains neutral with regard to jurisdictional claims in published maps and institutional affiliations.

**Open Access** This article is licensed under a Creative Commons Attribution 4.0 International License, which permits use, sharing, adaptation, distribution and reproduction in any medium or format, as long as you give appropriate credit to the original author(s) and the source, provide a link to the Creative Commons license, and indicate if changes were made. The images or other third party material in this article are included in the article's Creative Commons license, unless indicated otherwise in a credit line to the material. If material is not included in the article's Creative Commons license and your intended use is not permitted by statutory regulation or exceeds the permitted use, you will need to obtain permission directly from the copyright holder. To view a copy of this license, visit <http://creativecommons.org/licenses/by/4.0/>.

## References

- Bakeland LH. The chemical constitution of resinous phenolic condensation products. *J Ind Eng Chem.* 1913;5:506–11.
- Grosch KA. The relation between the friction and visco-elastic properties of rubber. *Proc R Soc Lond A.* 1963;274:21–39.
- Gong JP, Katsuyama Y, Kurokawa T, Osada Y. Double-network hydrogels with extremely high mechanical strength. *Adv Mater.* 2003;15:1155–8.
- Okata S, Hoshina K, Hanada K, Kamata H, Fujisawa A, Yoshikawa Y, et al. Hemostatic capability of a novel tetra- polyethylene glycol hydrogel. *Ann Vasc Surg.* 2022;84:398–404.
- Wichterle O, Lim D. Hydrophilic gels for biological use. *Nature.* 1960;185:117–8.
- Eu Patent 584,826B1.
- Horinouchi A, Atarashi H, Fujii Y, Tanaka K. Dynamics of water-induced surface reorganization in poly(methyl methacrylate) films. *Macromolecules.* 2012;45:4638–42.
- Tanaka M, Hayashi T, Morita S. The role of water molecules at the biointerface of medical polymers. *Polym J.* 2013;45:701–10.
- Singh S, Satani D, Patel A, Vhankade R. Colored cosmetic contact lenses: an unsafe trend in the younger generation. *Cornea.* 2012;31:777–9.
- Ortiz C, Jiménez R. Optical quality and vision with iris-coloring soft contact lenses. *Optom Vis Sci.* 2014;91:564–9.
- Efron, N *Contact lens practice.* 3 ed. (Elsevier, Netherlands 2017).
- US Patent US7048375 B2.
- Mahittikorn A, Kittichathanakul T, To-Im J, Nacapunchai D. Knowledge, behavior, and free-living amoebae contamination of cosmetic contact lens among university wearers in Thailand: a cross-sectional study. *Eye Contact Lens.* 2017;43:81–88.
- Bourcier T, Sauer A. Cosmetic contact lenses related microbial keratitis as a foreseeable disaster: a prospective study. *Invest Ophthalmol Vis Sci.* 2010;51:2884.
- Hong S, Lee JR, Lim T. Pigment deposition of cosmetic contact lenses on the cornea after intense pulsed-light treatment. *J Korean Ophthalmol.* 2010;24:367–70.
- Chan KY, Cho P, Boost M. Microbial adherence to cosmetic contact lenses. *Cont Lens Anterior Eye.* 2014;37:267–722.
- National Consumer Affairs Center, Japan Press Release, May 22, 2014.
- Stergiopoulou T, Meletiadiis J, Sein T, Papaioannidou P, Tsiouris I, Roilides E. Isobolographic analysis of pharmacodynamic interactions between antifungal agents and ciprofloxacin against *Candida albicans* and *Aspergillus fumigatus*. *Antimicrob Agents Chemother.* 2008;52:2196–204.
- Hotta F, Eguchi H, Imai S, Miyamoto T, Mitamura-Aizawa S, Mitamura Y. Scanning electron microscopy findings with energy-dispersive x-ray investigations of cosmetically tinted contact lenses. *Eye Contact Lens.* 2015;41:291–6.
- Jung JW, Han SH, Kim SA, Kim EK, Seo KY. Evaluation of pigment location in tinted soft contact lenses. *Cont Lens Anterior Eye.* 2016;39:210–6.
- Lorenz KO, Kakkassery J, Boree D, Pinto D. Atomic force microscopy and scanning electron microscopy analysis of daily disposable limbal ring contact lenses. *Clin Exp Optom.* 2014;97:411–7.
- Ito E, Takase H, Yamamoto K. TEM observation of inorganic substances distributed in gel materials for medical devices using ultra-thin cryosectioning. *Microscopy.* 2020;69:408–10.
- Ito E, Ohara A, Matsushita R, Yamamoto K. Analysis of distribution patterns of pigment in 3 classifications of color soft contact lenses. *J Jpn Cont Soc.* 2021;63:156–62.
- Yasuno S, Ishimaru S, Ikeno N. Relative sensitivity factors in hard X-ray photoelectron spectroscopy. *Surf Interface Anal.* 2018;50:1191–4.
- Cui YT, Tougaard S, Oji H, Son JY, Sakamoto Y, Matsumoto T, et al. Thickness and structure of thin films determined by background analysis in hard X-ray photoelectron spectroscopy. *J Appl Phys.* 2017;121:225307–10.
- Oji H, Matsumoto T, Cui YT, Son JY. An automated HAXPES measurement system with user-friendly GUI for R4000-10 keV at BL46XU in SPring-8. *J Phys Conf Ser.* 2014;502:012005.
- Kobayashi K. High-resolution hard X-ray photoelectron spectroscopy: application of valence band and core-level spectroscopy to materials science. *Nucl Instrum Methods Phys Res, Sect B.* 2005;547:98–112.

28. Rubio-Zuazo J, Castro GR. Non-destructive compositional depth profile analysis by hard x-ray photoelectron spectroscopy. *J Phys Conf Ser.* 2008;100:012042.
29. Bearden JA, Burr AF. Reevaluation of X-ray atomic energy levels. *Rev Mod Phys.* 1967;30:125–42.
30. Chen LX, Rajh T, Wang Z, Thurnauer MC. XAFS studies of surface structures of TiO<sub>2</sub> nanoparticles and photocatalytic reduction of metal ions. *J Phys Chem B.* 1997;101:10688–97.
31. Takahashi M, Watanabe I, Harada M, Mizoguchi Y, Miyanaga T, Yanase E, et al. Conversion electron yield XAFS for ceramics and metal alloys. *J Soc Mat Sci Jpn.* 1999;48:559–65.
32. Izumi A, Shudo Y, Kakara T. XAFS and HAXPES analyses of the oxidation state of a copper surface buried under a phenolic resin nanofilm. *Appl Surf Sci.* 2022;589:152967\_1–5.
33. ISO 18369-1 Ophthalmic optics - Contact lenses - Part 1: Vocabulary, Classification system and recommendations for labelling specifications. (2017).
34. Nojima S, Shinohara T, Higaki Y, Ishige R, Ohishi T, Kobayashi D, et al. Precise characterization of outermost surface of crystalline-crystalline diblock copolymer thin films using synchrotron radiation soft X-ray photoelectron spectroscopy. *Polym J.* 2014;46:637–40.
35. Roberts RF, Allara DL, Pryde CA, Buchanan DNE, Hobbins ND. Mean free path for inelastic scattering of 1.2 keV electrons in thin poly(methylmethacrylate) films. *Surf Interface Anal.* 1980;2:5–10.
36. Shinotsuka H, Tamuna S, Powwell CJ. Calculations of electron inelastic mean free paths. XIII. Data for 14 organic compounds and water over the 50 eV to 200 keV range with the relativistic full Penn algorithm. *Surf Interface Anal.* 2022;54:534–60.
37. Hong J, Totani M, Kawaguchi D, Yamada LN, Matsuno H, Tanaka K. Poly[oligo(2-ethyl-2-oxazoline) methacrylate] as a surface modifier for bioinertness. *Polym. J.* 2021;153:43–53.
38. Renault O, Martinez E, Zborowski C, Mann J, Inoue R, Newman J, et al. Analysis of buried interfaces in multilayer device structures with hard XPS (HAXPES) using a CrK $\alpha$  source. *Surf Interface Anal.* 2018;50:1158–62.
39. Shinotsuka H, Tamuna S, Powwell CJ, Penn DR. Calculations of electron inelastic mean free paths. XII. Data for 42 inorganic compounds and water over the 50 eV to 200 keV range with the relativistic full Penn algorithm. *Surf Interface Anal.* 2019;51:427–57.
40. Fuentes GG, Elizalde E, Yubero F, Sanz JM. Electron inelastic mean free path for Ti, TiC, TiN and TiO<sub>2</sub> as determined by quantitative reflection electron energy-loss spectroscopy. *Surf Interface Anal.* 2002;33:230–37.
41. Farges F, Lefrère Y, Rossano S, Berthereau A, Calas G, Brown G.E Jr. The effect of redox state on the local structural environment of iron in silicate glasses: a combined XAFS spectroscopy, molecular dynamics, and bond valence study. *J Non Cryst Solids.* 2004;344:176–88.